High-field side scrape-off layer investigation: Plasma profiles and impurity screening behavior in near-double-null configurations

B. LaBombard [a,*], A.Q. Kuang [a], D. Brunner [a], I. Faust [a], R. Mumgaard [a], M.L. Reinke [b], J.L. Terry [a], J.W. Hughes [a], J. Walk [a], M. Chilenski [a], Y. Lin [a], E. Marmar [a], G. Wallace [a], D. Whyte [a], S. Wolfe [a], S. Wukitch [a]

[a] *MIT Plasma Science and Fusion Center, 175 Albany St., Cambridge, MA 02139, USA*
[b] *Oak Ridge National Laboratory, Oak Ridge, TN 37831, USA*

ABSTRACT

New experiments on Alcator C-Mod reveal that the favorable impurity screening characteristics of the high-field side (HFS) scrape-off layer (SOL), previously reported for single null geometries, is retained in double null configurations, despite the formation of an extremely thin SOL. In balanced double-null, nitrogen injected locally into the HFS SOL is better screened by a factor of 2.5 compared to the same injection into the low field side (LFS) SOL. This result is insensitive to plasma current and Greenwald fraction. Nitrogen injected into the HFS SOL is not as well screened (only a factor of 1.5 improvement over LFS) in *unbalanced* double-null discharges, when the primary divertor is in the direction of B×∇B. In this configuration, impurity 'plume' emission patterns indicate that an opposing $E \times B$ drift competes with the parallel impurity flow to the divertor. In balanced double-null plasmas, the dispersal pattern exhibits a dominant $E \times B$ motion. Unbalanced discharges with the primary divertor *opposite* the direction of B×∇B exhibit *excellent* HFS screening characteristics – a factor of 5 enhancement compared to LFS. These data support the idea that future tokamaks should locate all RF actuators and close-fitting wall structures on the HFS and employ near-double-null magnetic topologies, both to precisely control plasma conditions at the antenna/plasma interface and to maximally mitigate the impact of local impurity sources arising from plasma-material interactions.

1. Introduction

Fluctuation-induced cross-field transport in the high-field side (HFS) scrape-off layer (SOL) is extremely low compared to the low-field side (LFS) [1]. Consequently, in double-null configurations, HFS density and temperature profiles are very sharp and, unlike the LFS, there are no density 'shoulders' that extend out to impact first wall components, including RF actuators. In single-null configurations, this HFS/LFS transport asymmetry drives strong parallel plasma flows, which poloidally through the SOL of the plasma from LFS to HFS. The HFS SOL also exhibits very strong impurity screening behavior in single-null configurations. Previous experiments have shown that it takes an order-of-magnitude larger injection rate of nitrogen (N) at the HFS midplane compared to the LFS midplane to produce the same core N content [2]. The lack of

interchange turbulence on the 'good curvature' side of the torus is believed to be at least partly responsible for both of these features in the HFS SOL – the very sharp density and temperature profiles in double-null configurations and a reduced level of impurity cross-field diffusion, as implied by the excellent N screening properties. Lacking plasma turbulence on the HFS, one might expect that neoclassical transport governs the profiles, particularly in balanced double-null configurations. In this regard, it is interesting to consider how narrow HFS profiles might relate to narrow heat flux footprints found at the divertor target plates [3]. Neoclassical ion drift effects have been invoked to explain the width of the observed divertor heat flux footprints in single-null plasmas, their inverse scaling with poloidal magnetic field strength and relative insensitivity to major radius of the device [4]. Measurements of HFS profiles and an examination of dependencies on plasma conditions are therefore of interest.

Moreover, it has been proposed [5] that future tokamaks should be designed to take advantage of these remarkable characteristics

* Corresponding author.
E-mail address: labombard@psfc.mit.edu (B. LaBombard).

of the HFS SOL to solve plasma-material interaction and steady state plasma sustainment challenges – relocate all RF actuators and close-fitting wall structures to the HFS and provide a large plasma-wall gap for structures on the LFS. Near-double-null magnetic topologies can be used to provide precise external control of upper/lower x-point flux-balance and HFS plasma-wall gap. In this way, plasma conditions at the HFS antenna/plasma interface could be tailored – even dynamically, in response to real-time measurements – both to optimize wave coupling and to minimize the level of plasma-material interactions. In addition, if the favorable HFS screening characteristics seen in single-null discharges also applied to near-double null configurations, the impact of impurities generated from plasma-wall interactions (possibly now controlled and reduced) would be further mitigated. These ideas are particularly compelling because theory and simulations indicate that RF wave accessibility and damping may be dramatically improved with HFS launch: lower hybrid waves can penetrate to mid minor radius (critical for current profile control) and a 40% or more increase in current drive efficiency may be obtained [6–9] (critical for reducing circulating power and obtaining net electricity production from fusion). In addition, there is a host of other potential benefits: energetic particle loads, ELM heat pulses and runaway electron damage on launch structures may be practically eliminated; neutron fluxes to RF launch structures may be minimized, particularly for locations above or below the inner midplane, which is synergistic with optimization of LHCD ray trajectories; thin, quiescent SOL minimizes undesirable interactions with SOL (e.g., wave scattering, collisional absorption, parametric decay instabilities); low plasma recycling fluxes lead to low neutral pressures and increased RF voltage limits. High field side ion cyclotron RF heating systems would also benefit from these attributes as well as exploit highly favorable wave physics [10], such as 100% first pass absorption of fast waves via mode conversion.

Motivated by this vision, the Alcator C-Mod team is presently investigating key aspects of HFS SOL physics in more detail: (1) Does the previously observed HFS impurity screening behavior extend to balanced double-null conditions where strong parallel flows to the divertor become relatively stagnant and the SOL profiles become very narrow? Could it be that such effects enhance HFS impurity penetration to the point where near balanced double null is a *disadvantage* with regard to core plasma impurity control? (2) How do the 'near SOL' profiles compare, HFS vs. LFS, particularly in balanced double-null? What does this information say about the physics that sets the near SOL widths?

This paper presents a snapshot of results from an ongoing investigation. The data presented here were obtained during Alcator C-Mod's 2015 run campaign in which HFS/LFS nitrogen screening characteristics of L-mode discharges were studied. The investigation will be extended to include H-mode and I-mode discharges before the end of Alcator C-Mod's final operation in 2016.

Sections 2–4 describe the experimental arrangement, the technique used to quantify the screening and nitrogen impurity ion source profile estimates. Section 5 presents experimental results for a range of magnetic equilibria, spanning upper-single null, balanced double null and lower-single null. Section 6 presents impurity 'plume' observations, which provide insight on the mechanisms that control impurity screening in the HFS SOL. High spatial resolution profile measurements, HFS and LFS, for balanced double-null plasmas at three values of plasma current are presented in Section 7. These examine the HFS-LFS mapping of the 'narrow feature' seen near the last-closed flux surface (LCFS). Section 8 discusses the principle findings of this work and its implications.
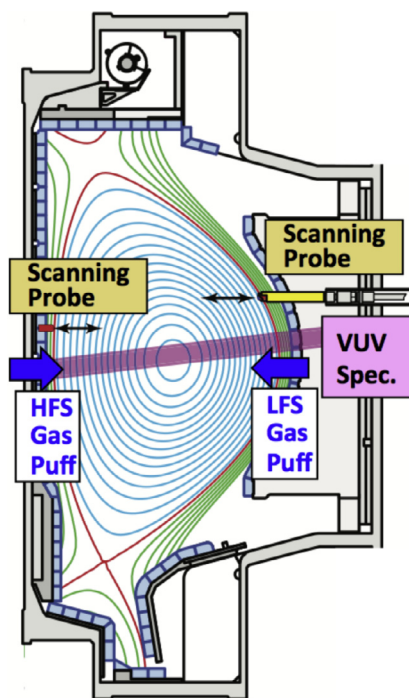

Fig. 1. Arrangement of HFS and LFS scanning probes, capillary 'gas puff' injectors, and the viewing chord for a vacuum ultraviolet spectrometer.

2. Experimental arrangement

Alcator C-Mod [11] is ideally suited for exploring HFS/LFS SOL profiles and impurity screening physics, employing an excellent plasma diagnostics suite that includes scanning probes and capillary gas injectors located on both the HFS and LFS midplanes (Fig. 1), a vacuum ultraviolet (VUV) spectrometer to monitor core plasma impurity emission (Fig. 1). In addition, visible light cameras (Figs. 7, 8) and a poloidally resolved, UV enhanced photodiode array (Fig. 9) are used to monitor nitrogen line emission from impurity 'plumes' that arise from local gas injections.

The two Langmuir-Mach scanning probes employ a four-electrode, high heat flux, pyramidal geometry [12]. These systems provide high-resolution profile measurements of density, electron temperature and parallel plasma flow up to and slightly inside the last closed flux surface (LCFS). Data from the HFS scanning probe electrodes (5 cm above the inner midplane) are obtained by fitting current-voltage characteristics generated by a 2 kHz triangular voltage sweep [1]. The LFS scanning probe (11 cm above outer midplane) employs a 'mirror Langmuir probe' (MLP) bias system [13, 14], producing measurements of density, electron temperature and parallel plasma flow at 1.1 MHz. For the plasmas reported here, nitrogen gas was introduced at HFS or LFS midplane locations via a capillary injection system [15]. An X-ray Extended Ultraviolet Spectrometer (XEUS) [16] with a central viewing chord (see Fig. 1) was used to monitor the brightness of NVI and NVII line emission over the spectral bands of 2.85–2.98 nm and 2.45–2.52 nm respectively. These signals are taken as a relative measure of the concentrations of N^{5+} and N^{6+} in the plasma core for otherwise identical discharges in which location and/or magnitude of the nitrogen gas puff is changed.

Calibrated nitrogen injections were performed on 45 L-mode plasmas (5.4 T, $B \times \nabla B$ towards lower x-point), spanning a variation in magnetic x-point balance (Fig. 2) at fixed current and density, a factor of two variation in plasma current (0.55, 0.8, 1.1 MA) at fixed Greenwald fraction (i.e., line-averaged density normalized to the Greenwald density [17]) and factor of two variation in Green-
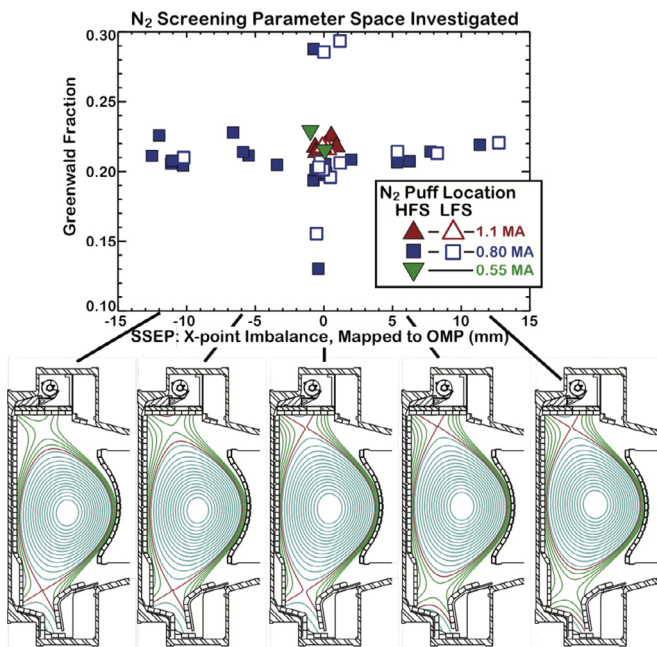
Fig. 2. The SOL screening characteristics of 45 L-mode discharges were investigated with the values of Greenwald fraction, plasma current and magnetic topology shown. Upper/lower x-point imbalance is parameterized by the difference in major radius at the outer midplane of their poloidal flux surface mappings.

Fig. 3. N5+ and N6+ line brightness signals (top two panels, red) in response to a nitrogen puff from the HFS midplane location (bottom panel). The signal responses are proportional to N2 flow rate, as demonstrated by overlays of this signal multiplied by the appropriate scale factors (blue). (For interpretation of the references to colour in this figure legend, the reader is referred to the web version of this article.)

wald fraction at fixed current (0.13 to 0.29). To facilitate a direct comparison of HFS versus LFS screening characteristics, identical plasmas were repeated in many cases, changing HFS/LFS nitrogen injection location.
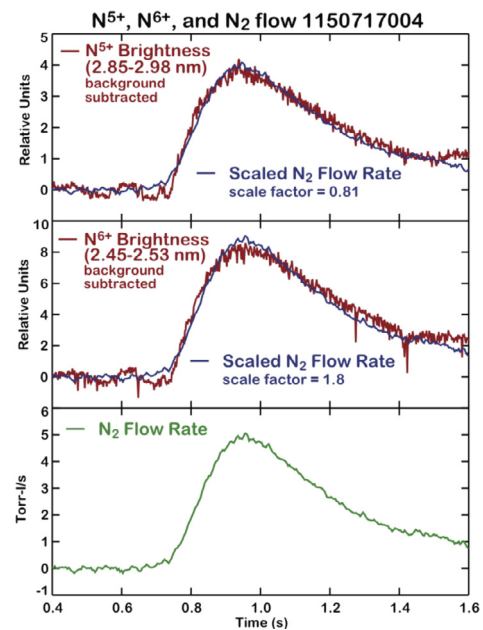
3. Method used to measure impurity penetration factor

Nitrogen behaves as a weak-recycling, non-intrinsic impurity species in Alcator C-Mod [2] and therefore may be employed as a trace impurity to investigate screening characteristics of the HFS and LFS scrape-off layers. In response to a nitrogen source introduced at the first wall, the number of nitrogen ions in the confined plasma region (N_N) may be expressed as a flux balance equation, applied at the LCFS interface,

$$\frac{\partial N_N}{\partial t} = PF \ \Gamma_N - \frac{N_N}{\tau_p}. \tag{1}$$

In this highly simplified model, nitrogen gas injected at the first wall at the rate Γ_N (#/s) first becomes ionized in the SOL and then a fraction of that impurity ion influx, $PF \ \Gamma_N$ manages to cross the LCFS into the confined plasma region. In this context, PF is an 'impurity penetration factor', which encapsulates the 'screening' characteristics of the SOL and τ_p is the characteristic confinement time for nitrogen impurities in the core; lacking any external source of nitrogen ions, N_N would decay at this characteristic time. It is conceptually helpful to think of τ_p as being independent of impurity injection location, although it need not be (more on that below). [Note: the definition of penetration factor used here differs from that defined by McCracken, which had units of s^{-1}.] The physics that determines PF is, of course, very complex involving: (1) the location in which the impurities are ionized in the SOL, (2) cross-field transport ($E \times B$ drifts, diffusion, convective 'pinches') and (3) the residence time of nitrogen impurities ions in the SOL, which should not be confused with τ_p. See ref [18] for a more complete treatment of this topic.

In quasi-steady state, $|\frac{\partial N_N}{\partial t}| \ll \frac{N_N}{\tau_p}$, the number of nitrogen ions in the confined plasma region becomes $N_N = PF \ \Gamma_N \tau_p$. When $PF = 1$,

the SOL provides no screening at all; the full flux of wall-source impurities makes it into the confined plasma. Thus the purity of the core plasma is critically dependent on the impurity screening characteristics of the SOL. It is highly desirable to identify operational scenarios and/or external control techniques in which PF can be made as small as possible, particularly at locations in which intrinsic impurity sources are known to exist.

If nitrogen truly behaves as a non-recycling impurity, then recycling does not contribute to Γ_N. In this case, Γ_N is the externally imposed gas puff and PF corresponds to the SOL impurity screening at the point of injection. Moreover, if $|\frac{\partial N_N}{\partial t}| \ll \frac{N_N}{\tau_p}$ is satisfied and τ_p is not varying in time, then the core plasma nitrogen content should be strictly proportional to the external injection rate. Fig. 3 shows the time behavior of core plasma nitrogen brightness signals (red traces) in response to a nitrogen gas puff from the HFS midplane. Background signal levels measured just before the gas injection are subtracted. The N2 gas injection rate is shown in the bottom panel. The blue traces in the top two panels are N2 gas injection rate, multiplied by appropriate scale factors so to make these traces overlay with the brightness signals. One can see that the core nitrogen content is indeed proportional to the nitrogen puff rate. The scale factors deduced are therefore a measure of the impurity screening characteristics of the local SOL,

$$Scale \ Factor \propto \frac{N_N}{\Gamma_N} = PF \ \tau_p. \tag{2}$$

By injecting nitrogen gas from HFS and LFS midplanes in otherwise identical plasmas, one can directly deduce the ratio of impurity penetration factors – it is the ratio of the scale factors needed to align gas puff and nitrogen line emission brightnesses. Moreover, in the case that the core impurity confinement time depends on impurity injection location, the ratio of scale factors is more generally as a measure of the relative contamination efficiency, $CF = PF \ \tau_p$,

$$\frac{Scale \ Factor|_{HFS}}{Scale \ Factor|_{LFS}} \propto \frac{(PF \ \tau_p \ )_{HFS}}{(PF \ \tau_p \ )_{LFS}} = \frac{CF_{HFS}}{CF_{LFS}}. \tag{3}$$
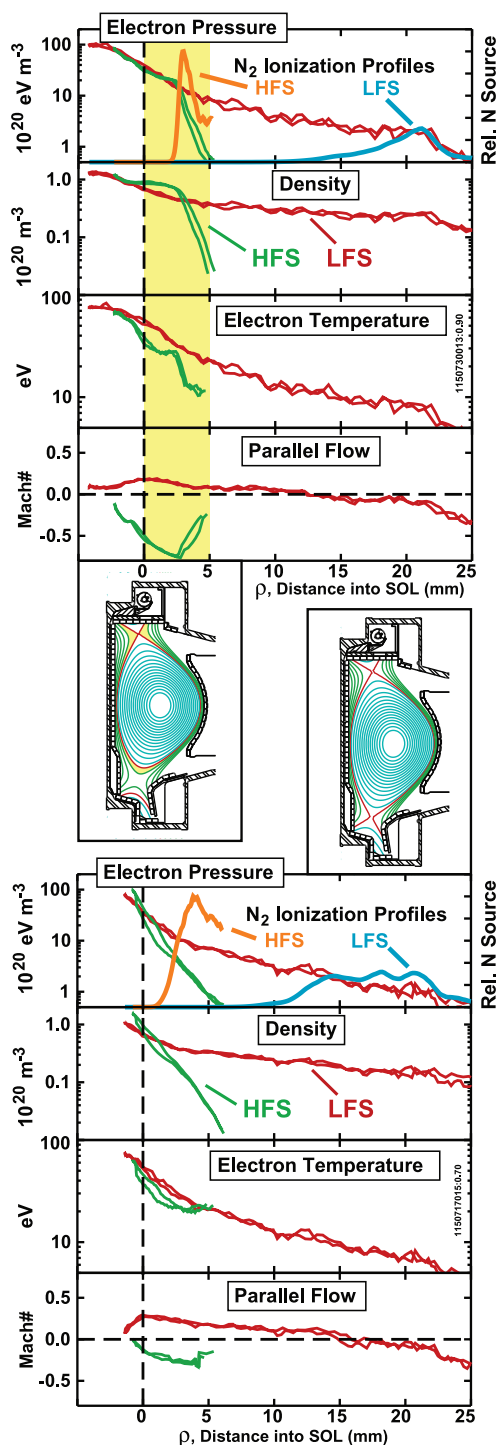
Fig. 4. Electron pressure, density, electron temperature and parallel flow Mach number profiles for an unbalanced, upper-null dominant equilibrium (top) and a balanced double-null equilibrium (bottom). The spatial region in which SOL flux surfaces are common to HFS and LFS are highlighted in yellow. Positive Mach number is flow in the direction of B – towards the divertor on LFS and away from the divertor on HFS. Estimated ionization source profiles are shown for HFS (orange) and LFS (cyan) nitrogen injection cases. (For interpretation of the references to colour in this figure legend, the reader is referred to the web version of this article.)

This is the technique used to quantify the relative impurity screening responses (or contamination efficiencies) reported in this paper.

N^{5+} and N^{6+} brightness signals are found to be approximately proportional to each other and therefore yield essentially identical results in terms of computing a scale factor ratio from Eq. (3).

However, a better signal-to-noise ratio obtained from the N^{6+} brightness data. Therefore, we report scale factors deduced from the ratio of N^{6+} brightness to gas puff injection rate for all discharges investigated (Section 5). We normalize them so that this relative penetration factor is unity for the case of a LFS nitrogen injection into a 0.8 MA balanced double-null plasma with Greenwald fraction of 0.2

4. Effect of magnetic topology on SOL profiles and nitrogen ionization source location

The effect of x-point balance on HFS and LFS scrape-off layer profiles has been well documented on Alcator C-Mod [1, 19–21]. As the magnetic topology is changed from single-null to double-null, density and temperature profiles in the HFS scrape-off layer develop a very sharp exponential decay at the location in which the poloidal magnetic flux surfaces become 'private' to the HFS region. Using the HFS/LFS scanning probes (details on the scanning probe data analysis is described in Section 7), the effect was revisited for selected discharges in the data set. Fig. 4 shows results from two otherwise identical discharges in the data set (0.8 MA, Greenwald fraction 0.2) – an unbalanced, upper null dominant discharge (top panel), with distance between primary and secondary separatrices of ∼5 mm mapped to the outer midplane, and a balanced double-null plasma (lower panels). In the upper-null dominant case, HFS/LFS electron pressure profiles approximately match, out to the radial location where the SOL flux surfaces contains the secondary x-point (yellow shaded region). Electron pressure and density profiles exhibit a very sharp density decay beyond that point. Parallel flow Mach numbers on the HFS are very large, approaching 0.8 directed towards the inner strikepoint of the upper divertor.

In contrast, for the balanced double null case, profiles on the HFS and LFS SOLs match only at the LCFS. The sharp decay in the HFS profiles begins immediately at the LCFS. Parallel flow Mach numbers on the HFS are reduced in this case, with a maximum value of 0.2 directed toward the upper divertor.

Based on the measured density and electron temperature profiles, it is informative to estimate the nitrogen ionization source profiles, $S(r)$, resulting from a flux of nitrogen molecules originating at the first-wall (Γ_0), both from HFS and LFS. This is shown on Fig. 4 as orange traces for the HFS case and cyan traces for the LFS case. This estimate considers the spatial attenuation of Γ_0 (at wall temperature) due to N_2 ionization and computes the resultant N source profile based on its spatial derivative,

$$S(r) = \frac{\partial \Gamma_{N_2}}{\partial r} = \Gamma_0 \frac{\partial}{\partial r}\left\{ \exp\left(-\int_0^r \frac{n_e}{v_0}\langle \sigma v \rangle \partial r \right) \right\}. \quad (4)$$

From Fig. 4, one can see that the spatial location of the N source profiles HFS versus LFS is dramatically different, moving ∼1 cm closer to the LCFS for the HFS case. Changing from unbalanced double null to balanced double null produces a much smaller inward shift of the HFS nitrogen source profile.

Based on these considerations, one might expect the nitrogen screening of the HFS SOL to be much less effective as the magnetic topology is changed from single-null to balanced double null – the 'impurity flushing action' of the SOL parallel flow is reduced and the nitrogen ionization source moves very close to the LCFS. However, fluctuation-induced cross-field particle transport on the HFS SOL is extremely low, essentially zero according to direct measurements [1]. Thus a central question is: Does the very low level of cross-field impurity diffusion in the 'quiescent' HFS scrape-off layer provide adequate screening of wall-source impurities for the case of a balanced double-null discharge? Here an 'adequate' level of
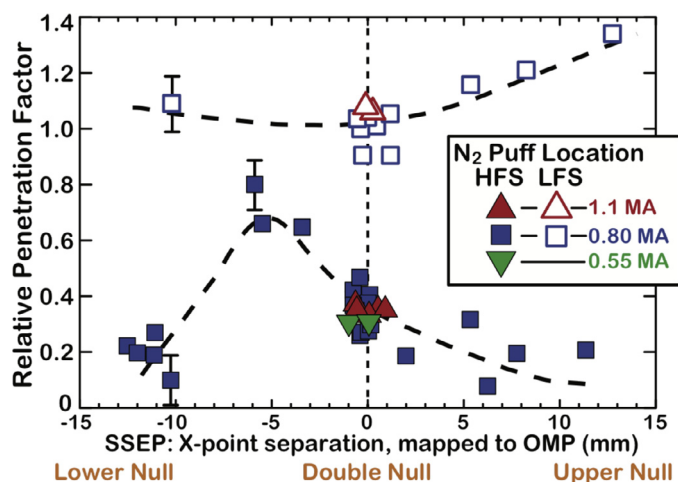
Fig. 5. Relative nitrogen penetration factor as a function of upper/lower x-point separation (SSEP). Dashed lines are added to guide the eye – these are not fits to the data.
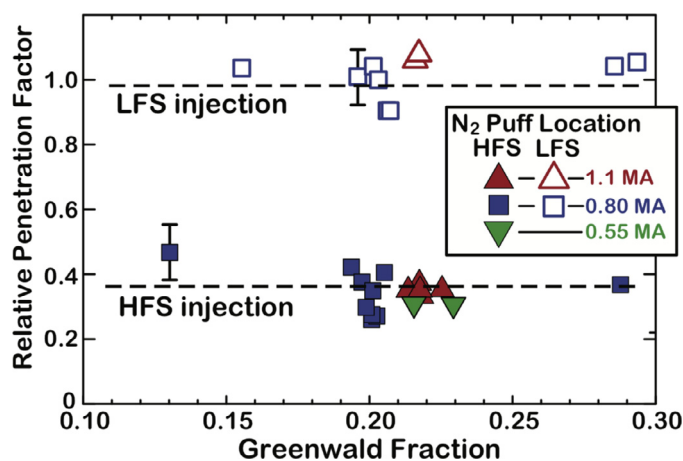

Fig. 6. Relative nitrogen penetration factor as a function of Greenwald fraction for balanced double-null discharges.

impurity screening might be at a level that is comparable or better than that observed for the LFS SOL.

5. Experimental results: HFS/LFS nitrogen penetration factors

Relative nitrogen penetration factors are shown in Fig. 5 for the full set of 45 L-mode discharges. The data are ordered according to upper/lower magnetic flux surface balance, which is parameterized as the x-point separation distance when mapped along poloidal flux surfaces to the outer midplane (SSEP). The penetration factors are normalized to the value obtained for a LFS injection into a 0.8 MA balanced double-null plasma with Greenwald fraction of 0.2. Based on the quality of the fit between gas flow rate and N^{+6} line brightnesses (see Fig. 3 as an example) we estimate the vertical error bars on the data points in Figs. 5 and 6 to be as shown. This is consistent with the discharge-to-discharge scatter in these measurements.

Remarkably, nitrogen impurity penetration factors on the HFS SOL are persistently lower than the LFS SOL, despite extremely narrow HFS profiles (Figs. 4 and 10). For balanced double null configurations, the HFS impurity penetration is a factor of 2.5 lower then LFS. This remains true for a factor of 2 variation in plasma current at fixed Greenwald fraction and a factor of two variation in Greenwald fraction at fixed plasma current (Fig. 6). As SSEP is increased to large positive or large negative values, HFS nitrogen impurity

penetration becomes a factor of ~10 lower than LFS. This is consistent with previous observations of LFS discharges [2] in which SSEP values of −20 mm or less where employed.

Although it is expected that HFS impurity penetration factors should increase as the magnetic topology moves toward double-null plasma, it is perhaps unexpected that balanced double-null plasmas (SSEP ~0 mm) do not produce the highest impurity penetration factors. Instead, the maximum HFS penetration factor is found for *unbalanced* double-null plasmas, with SSEP values around −5 mm. This offset cannot be simply attributed to errors in magnetic flux surface reconstruction because the HFS/LFS scanning probe profile data are found consistent with the SSEP values, i.e., when SSEP is near zero, the HFS scanning probe reports a sharp fall-off in the SOL, roughly coincident with the location of the LCFS (Fig. 10), i.e., there is no 'shoulder' in the HFS SOL that maps between HFS and LFS to indicate the presence of a zone of common poloidal flux. For unbalanced double-null plasmas with SSEP around +5 mm, the HFS nitrogen screening is exceptional, approaching a factor of ~10 improvement relative to the LFS.

A possible explanation for the offset peak in nitrogen penetration factor comes from recognizing that plasma flow in the SOL includes both parallel and perpendicular ($E \times B$) components; the overall rate that impurities are flushed to the divertor depends on whether these flows work together or in opposition. Due to the tight coupling between electron temperature and potential profile in the SOL, the radial electric field tends to point in the direction of minor radius. Thus when B×∇B points away from the dominant divertor, both $E \times B$ and parallel flow on the HFS can be directed toward that divertor. When B×∇B points toward the dominant divertor, it is possible that the poloidal projections of $E \times B$ and parallel flows oppose; the impurity flushing action becomes reduced or stagnant. This idea was investigated by looking at the nitrogen impurity 'plume' dispersal patterns with visible cameras and a poloidally-resolved Lyman-alpha photodiode array. Note that in principle the plasma potential profiles and resultant $E \times B$ flow can be deduced from HFS scanning probe data. However, we have found such measurements to be noisy and unreliable. Moreover, since nitrogen concentration profile in the SOL is unknown, one does not know where to evaluate the $E \times B$ flow. Looking at the plume dispersal pattern avoids these problems. It tells us exactly what we want to know: where the impurities are going.

6. Nitrogen 'plume' dispersal observations

6.1. "Maypole plume"

In the process of setting up the HFS/LFS screening experiments, some lower single-null plasmas where run (SSEP < −20 mm) with a large gas puff applied to the HFS midplane capillary. This resulted in a 'maypole plume' – a field-aligned plume of emission on visible light cameras that wrapped around the center stack down to the lower divertor (Fig. 7). This observation clearly illustrates the 'quiescent' nature of the HFS SOL – it is essentially a laminar flow of nitrogen impurities that extends for a very long distance (~ 4 m) compared to the SOL width (few mm) – and the strong role that HFS parallel flows can play in flushing HFS impurities toward the divertor. In this topology, parallel Mach numbers on the HFS can approach unity in the far SOL [19]. In contrast, no such streamers are observed when nitrogen is puffed at the LFS midplane.

6.2. Effect of upper/lower x-point balance on plume dispersal pattern

Using the 'front camera' view of Fig. 7, the HFS nitrogen impurity dispersal patterns were examined for balanced and slightly unbalanced double null plasmas, in particular, the condition (SSEP ~ −5 mm) when HFS injection produces the highest penetration
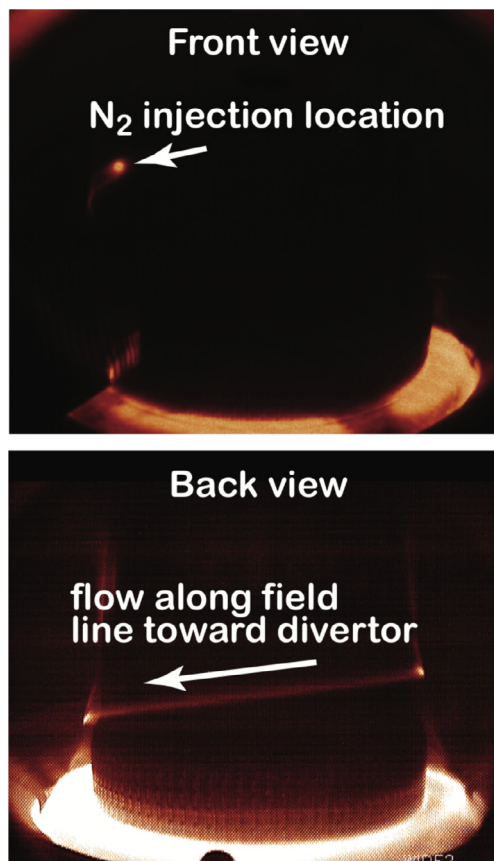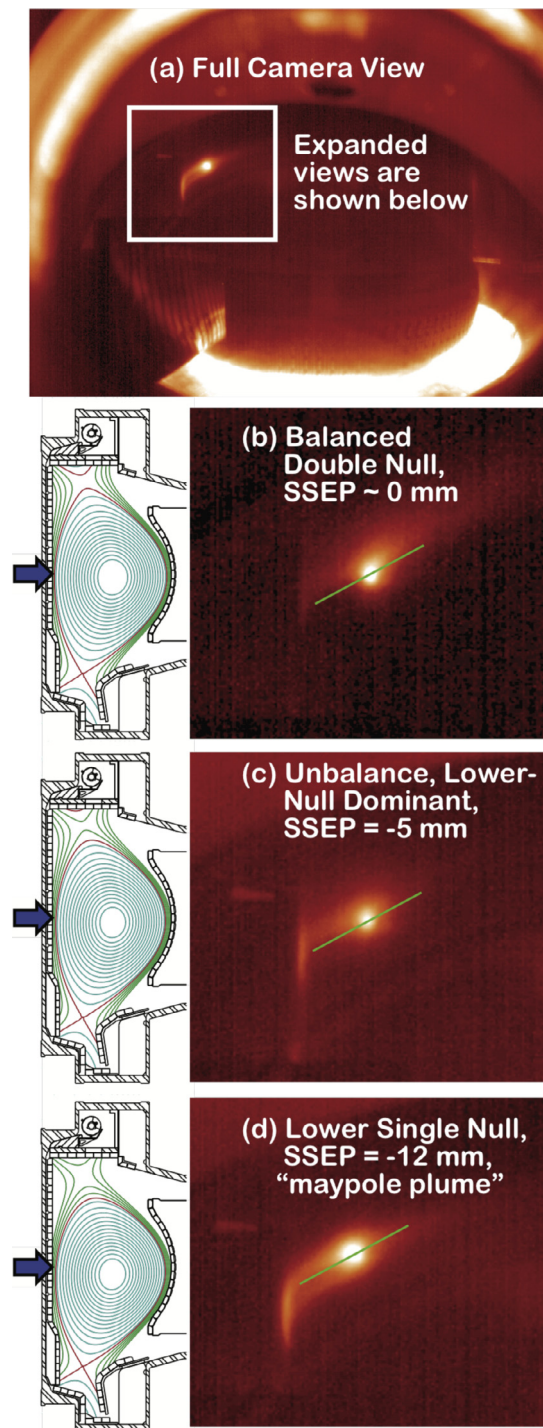
Fig. 7. A 'maypole plume,' observed in unfiltered visible light emission (false color image is shown) for a lower single-null plasma with strong nitrogen puff from an inner-wall midplane capillary tube, directly illustrates strong parallel flows to the divertor and the 'quiescent' nature of the HFS SOL.

Fig. 8. Camera images of nitrogen injection plume: (a) upper single null, (b) balanced double-null, (c) unbalanced, lower null dominant, and (d) lower single null magnetic configurations.

factors. Fig. 8 shows cases of (b) balanced double null, (c) unbalanced double null (SSEP ~ -5 mm), and (d) lower single null (SSEP ~ -12 mm). The corresponding magnetic equilibria are also shown. Case (d), lower single null, has the same magnetic equilibrium as the 'maypole plume' case shown in Fig. 7 but the nitrogen flow rate is reduced by about a factor of two to a level that is similar to cases (b) and (c). To guide the eye, a green line is drawn on panel (d), aligned, orientated with the plume streamer. A green line with the same orientation is shown on panels (b) and (c).

The plume dispersion pattern in balanced double null, panel (b), does not suggest a preferred flow direction along the magnetic field line. This 'boomerang' pattern [22] is indicative of spreading in both directions along magnetic field lines combined with a strong $E \times B$ a drift toward the upper divertor. The plume dispersal pattern for the unbalance, lower-null dominant case (SSEP ~ -5 mm) does show evidence of a directed flow, but the stream is not field-aligned; it appears to be drifting ($E \times B$) toward the upper divertor as it moves along field lines. The net result is that the impurity streamer circles around the center stack, with little or no directed motion towards either divertor.

Further information on the nitrogen plume dispersal was obtained from an array of bandpass filtered photodiodes (Fig. 9) that view UV emission in the Ly$_\alpha$ wavelength range (120 nm center, 8.6 nm FWHM) along horizontal chords at different elevations. This system is normally used to assess hydrogenic ionization in the boundary plasma. However, this spectral band has been found to be an excellent monitor for the concentration of N^{4+} ions, taking advantage of bright 2p-2s lines at 123.88 and 124.28 nm [23].

The diode array is at the same toroidal location as the HFS nitrogen injection capillary, with chord number 13 (see Fig. 9) viewing the gas puff capillary. Profiles of photodiode voltage data are shown for four magnetic configurations in which a HFS gas puff was applied: (a) upper single null, (b) balanced double-null, (c) unbalanced, lower null dominant, and (d) lower single null. (Data from chords 1–6 are unreliable and therefore not shown.) The overlaid profiles for each case track the change ion photodiode signal from the beginning of the gas puff to when a steady nitrogen flow
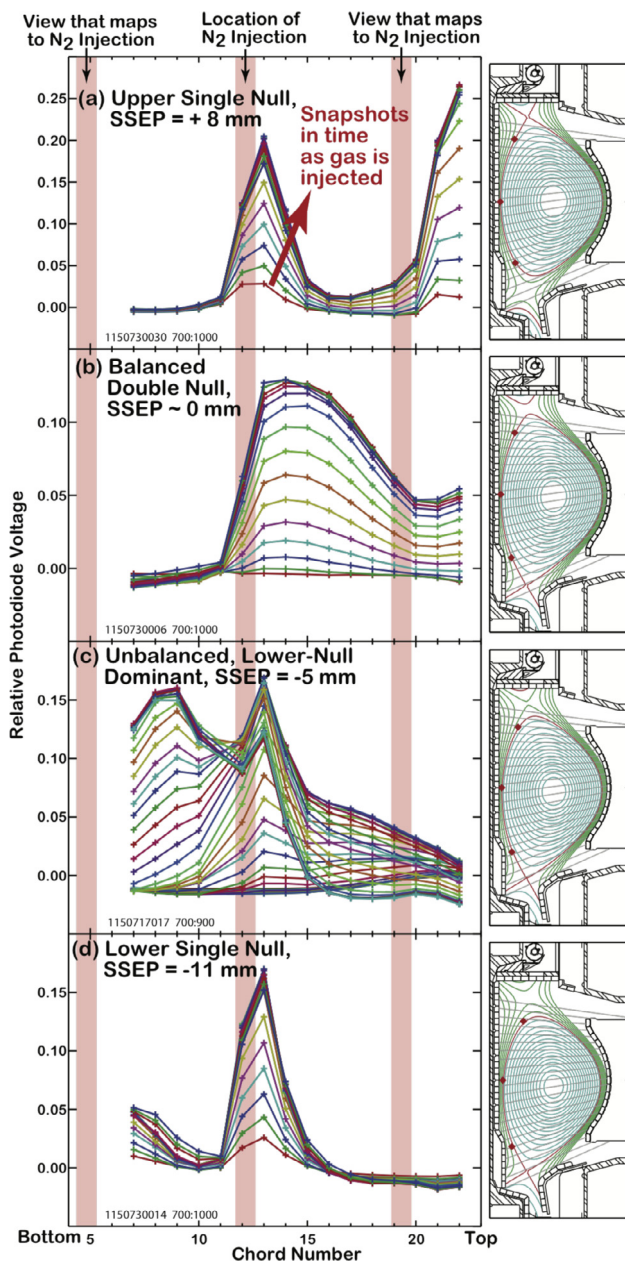
Fig. 9. Ly_α photodiode array measurements of HFS nitrogen injection plume for (a) upper single null, (b) balanced double-null, (c) unbalanced, lower null dominant, and (d) lower single null magnetic configurations. Chord #13 views the location of the nitrogen gas puff. Red symbols on equilibrium plots (right panels) indicate where a magnetic field line that starts at the gas puff location passes in front of the diode array as it wraps around the torus. These locations are also indicated as vertical red bands on the photodiode data (left panels). Overlaid profile 'snapshots' show the time evolution, starting from when the gas puff is turned on to when the peak flow rate is approached. Baseline signal levels are subtracted, corresponding to a 100 msec time average taken before the puff. (For interpretation of the references to colour in this figure legend, the reader is referred to the web version of this article.)

is established. For all cases, a strong signal is seen on midplane chords near point of N_2 injection, albeit not centered about the point of injection. This central emission peak is shifted to higher elevations, with its prominence depending on magnetic equilibrium. A number of features are specific to each equilibrium can be noted:

a) *upper single null* – In this case the midplane peak is narrow and second peak appears at the highest elevation. The location

of the second peak does not correspond to a strict field line mapping (red vertical band) but appears above it. There is essentially no emission below the inner midplane. The emission pattern is consistent with a field-aligned plume heading to the upper divertor, but perhaps with the assist of an upwards $E \times B$ drift.

b) *balanced double-null* – In this case the midplane peak is strongly skewed to toward the upper chamber. There is no emission below the inner midplane. This emission pattern is consistent with the 'boomerang' plume seen in Fig. 8b; it is indicative of a very strong $E \times B$ drift of the nitrogen impurities toward the upper divertor.

c) *unbalanced, lower null dominant* – A midplane peak is observed but the emission pattern is very broad, favoring an asymmetry towards the upper divertor early in time and an asymmetry towards the lower divertor late in time. The pattern late in time shows a second peak below the midplane. The location of this peak does not correspond to a strict field line mapping (red vertical band) but appears significantly above it. Early in time, this emission pattern hints at a strong upward drift, and later in time a field-aligned plume heading to the lower divertor, but with a strong upwards $E \times B$ contribution.

d) *lower single null* – In this case the midplane peak is narrow again and there is a hint of another peak occurring at the lowest elevation. The emission pattern is consistent with a field-aligned plume heading to the lower divertor, but perhaps with some upwards $E \times B$ contribution as well.

Taken together, these observations are strong evidence that both parallel and $E \times B$ flow contributions determine the total impurity dispersion and, by inference, the rate in which impurities are 'flushed' to the divertor. In this sense, the impurity dispersal pattern observed for the unbalanced, lower null dominant case (SSEP$=-5$ mm), is consistent with the HFS impurity penetration factor being maximum for this configuration – the penetration factor is largest primarily because the HFS SOL impurity residence time is the longest.

7. Comparison of HFS/LFS scrape-off layer profiles in balanced double-null

The HFS and LFS scanning probes were used to investigate profiles of density and electron temperature in balanced double-null configurations. Because of the high heat flux density in Alcator C-Mod SOL, placing tungsten electrodes at the LCFS without overheating or damaging them requires a careful trial-and-error optimization. Fig. 10 shows the best set of SOL profiles obtained thus far for three balanced double-null plasmas with fixed Greenwald fraction (0.21) and varied plasma current (0.55, 0.8, 1.1 MA). The green (HFS) and red (LFS) profile traces shown in Fig. 10 (and also Fig. 4) represent data obtained over the probe's inward and outwards trajectories, plotted as a function of flux surface coordinate, ρ, which is the distance into the SOL mapped to the outer midplane. Data obtained from inward and outward scans overlay well, indicating that the electrodes did not experience overheating or damage. An exception is for HFS measurements in the 1.1 MA case (rightmost panels) – the outgoing trace is not shown because the electrodes were inserted too deep and showed evidence of overheating (electron emission). The traces are obtained by processing the probe data in the following way. First the density or temperature values reported at each time step by the four electrodes are averaged together. Then these data are averaged over a running time window. For the HFS probe, this amounts to combining data obtained from fitting five I-V characteristics, corresponding to a 1.25 ms running time window. The LFS data are averaged over a time window of 0.2 ms, effectively consolidating data from 220 I-V
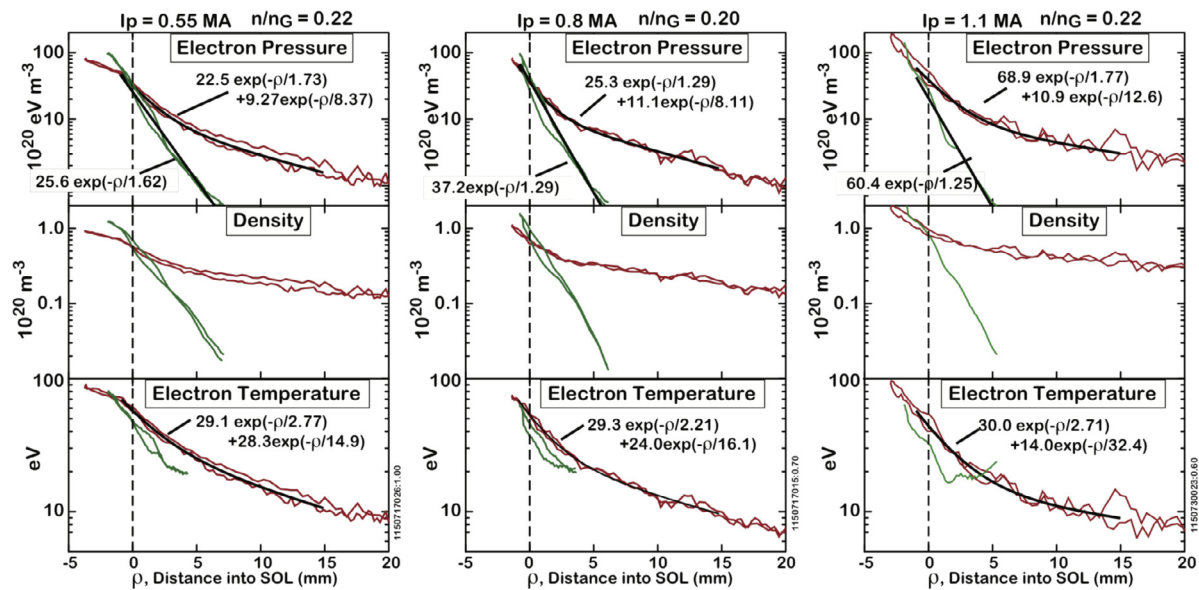
Fig. 10. Comparison of HFS and LFS SOL profiles in balanced double-null plasmas for three difference plasma currents and fixed Greenwald fraction. Data is shown plotted versus distance into the SOL mapped to the outer midplane. Note that LFS profile data are shifted in ρ by up to ~ 2 mm so as to 'align' $T_e \sim 50$–60 eV with the LCFS ($\rho = 0$). HFS profile data are shifted to 'align' electron pressure between LFS and HFS at the LCFS.

characteristics generated by the MLP three-point voltage bias system. Accounting for the maximum radial velocities of the probes, these time averages correspond to spatial averages of 0.7 mm and 0.38 mm, respectively. It should be noted that there is significant uncertainty and variability discharge-to-discharge in the mapping probe data to ρ-space, of order ~ 2 mm. On the other hand, based on power balance constraints, we expect that electron temperatures near the LCFS on the LFS should be in the range of 50 to 60 eV This is used as a rough guide to 'correct' and 'align' the LFS profiles relative to the LCFS. Then, based on the expectation that electron pressure should approximately match near the LCFS from LFS to HFS, this constraint is used as guide to 'align' the HFS profiles shown in Fig. 10.

A number of observations can be made based on the data shown in Fig. 10:

1. *Two zone LFS SOL* - LFS density and electron temperature profiles show a clear two-zone structure that is widely seen in tokamak experiments – a 'near SOL' with a sharp e-folding length and a 'far SOL' or 'shoulder' with a much longer e-folding length. The profile shapes are well described by a two-exponential fit. Electron pressure and electron temperature decay lengths deduced from fits are shown.
2. *Single zone HFS SOL* - HFS density and electron temperature profiles are extremely sharp compared to LFS. At a distance of 7 mm into the SOL, density in the HFS SOL drops by two orders of magnitude. (At this point in the profile, the signal is below the dynamic range of the diagnostic; electron temperatures deduced from I-V characteristics become unreliable and are therefore suppressed in Fig. 10). In contrast, density on the LFS drops by only a factor of 2 to 3. The sharp HFS electron pressure and density profile fall off is well described by a single exponential decay length. Fitted curves for electron pressure are shown.
3. *Near SOL maps between HFS and LFS* - The electron pressure e-folding lengths in the near SOL regions are essentially identical HFS vs LFS – and this single e-folding length applies for several e-folds into the HFS SOL.
4. Contrary to expectations, near SOL e-folding lengths do not indicate a strong dependence on plasma current.

These data clearly indicate that the primary difference between HFS and LFS profiles is the formation of a 'shoulder' feature in the LFS far scrape-off layer that is lacking on the HFS. The very sharp gradients that appear on the HFS in balanced double null configurations is essentially equivalent to the 'near SOL' or 'narrow heat flux feature' that is seen on the LFS. The fact that the narrow electron pressure e-folding length extends for a long distance into the HFS SOL is perhaps telling. Apparently, the transport physics that sets this scale length continues to apply over a region that is disconnected magnetically from the LFS SOL. It is therefore the scale length associated with a region of exclusively good curvature, with no interchange turbulence drive.

8. Summary and discussion

Impurity screening of the high-field side (HFS) scrape-off layer (SOL) to local nitrogen injection has been quantified relative to that of the low-field side (LFS) in Alcator C-Mod for L-mode plasmas that span a range of magnetic equilibria: upper single-null, balanced double-null and lower single-null. In addition, plasma density and temperature profiles on the HFS and LFS SOLs are measured in balanced double-null with high spatial resolution. This work was motivated by the following considerations: (1) previous experiments in Alcator C-Mod found that the screening of nitrogen impurity ions by the HFS SOL is a factor of ~ 10 better than that of the LFS SOL in single-null magnetic topologies [2], (2) solutions to first-wall and RF actuator plasma-material interaction challenges are critically needed in order to achieve sustained steady state plasma operation and (3) it has been proposed that future tokamaks should exploit the excellent screening and 'quiescent' nature of the HFS SOL – locate all RF actuators and close-fitting wall structures to the HFS and employ *near-double-null* magnetic topologies, to precisely control plasma conditions at the antenna/plasma interface, both to optimize wave coupling and to mitigate the impact of PMI [5]. In this regard, the present work was performed to answer the following important questions: does the previously observed HFS impurity screening behavior extend to *balanced double-null* conditions where strong parallel flows to the divertor become relatively stagnant and the SOL profiles become very narrow? Or, does SOL impurity screening become ineffective in balanced double-null

so as to spoil these ideas? How do HFS SOL profiles relate to LFS SOL profiles in balanced double null, particularly in the 'near SOL' regions?

Despite an extremely thin scrape-off layer on the HFS with very sharp n, T_e profiles in balanced double-null (Fig. 10), the HFS SOL is still found to be better at screening nitrogen than the LFS SOL by a factor of 2.5 (Fig. 5). This is very favorable for the idea of relocating RF actuators to the HFS. The electron plasma pressure e-folding lengths near the last closed flux surface are found to be essentially the same LFS and HFS. On the HFS, this e-folding length is maintained all the way out to first-wall contact while on the LFS SOL, the usual flattening of the pressure profile ('shoulders') is exhibited. Factors of two variation in plasma current and Greenwald fraction are found to have no influence on the HFS or LFS impurity screening behavior. Instead, upper/lower x-point balance is found to be the most important control parameter. Surprisingly, HFS impurity screening is least effective (only a factor of 1.5 better than LFS) for *unbalanced* double-null plasmas that favor the active divertor in the direction of $B \times \nabla B$. In this configuration, impurity 'plume' emission patterns indicate that an opposing $E \times B$ drift competes with impurity flow to the divertor along field lines. Consequently, nitrogen impurity residence time in the HFS SOL are likely maximized in this configuration. In balanced double-null plasmas, the dispersal pattern takes on a 'boomerang' shape, indicating a dispersal that is dominated by strong $E \times B$ drift motion. Unbalanced double-null discharges that favor the most active divertor *opposite* the direction of $B \times \nabla B$ have *excellent* HFS screening characteristics, a factor of 5 to 10 better than for LFS.

It should be noted that the latter situation is particularly promising for the use of HFS RF actuators in I-mode plasmas. I-mode is a confinement regime that is uniquely reactor-relevant – high confinement, steady, ELM-free – and it is accessible over a wide power range at high magnetic field, *particularly when the most active divertor is opposite the direction of* $B \times \nabla B$ [24]. Based on these results, we are highly motivated to extend this impurity screening investigation to H-mode and I-mode confinement regimes in near-balanced double null configurations before the end of Alcator C-Mod's final run campaign in 2016.

References

[1] N. Smick, B. LaBombard, I.H. Hutchinson, Nucl. Fusion 53 (2013) 023001.
[2] G.M. McCracken, et al., Phys. Plasmas 4 (1997) 1681.
[3] T. Eich, et al., Nucl. Fusion 53 (2013) 093031.
[4] R.J. Goldston, Nucl. Fusion 52 (2012) 013009 (7 pp).
[5] B. LaBombard, et al., Nucl. Fusion 55 (2015) 053020.
[6] Y.A. Podpaly, G.M. Olynyk, M.L. Garrett, P.T. Bonoli, D.G. Whyte, Fusion Eng. Des. 87 (2012) 215.
[7] B.N. Sorbom, et al., Fusion Eng. Des. 100 (2015) 378.
[8] G.M. Wallace, et al., Development of lower hybrid current drive actuators for reactor relevant conditions, presented at the 41st EPS Conference on Plasma Physics and Controlled Fusion, Berlin, Germany, 2014.
[9] G.M. Wallace, et al., High field side launch of lower hybrid waves: a scoping study for ADX, presented at the 26th IEEE Symposium on Fusion Engineering, Austin, TX, 2015.
[10] P.T. Bonoli, et al., Bull. Am. Phys. Soc. 59 (2014) 363.
[11] I.H. Hutchinson, et al., Phys. Plasmas 1 (1994) 1511.
[12] N. Smick, B. LaBombard, Rev. Sci. Instrum. 80 (2009) 023502.
[13] B. LaBombard, L. Lyons, Rev. Sci. Instrum. 78 (2007) 073501.
[14] B. LaBombard, et al., Phys. Plasmas 21 (2014) 056108.
[15] D. Jablonski, et al., J. Nucl. Mater. 241-243 (1997) 782.
[16] P. Beiersdorfer, J.K. Lepson, M. Bitter, K.W. Hill, L. Roquemore, Rev. Sci. Instrum. 79 (2008) 10E318.
[17] M. Greenwald, Plasma Phys. Control. Fusion 44 (2002) 27.
[18] P.C. Stangeby, The Plasma Boundary of Magnetic Fusion Devices, in: Peter C. Stangeby (Ed.), Institute of Physics Pub., Bristol, UK ; Philadelphia, PA, 2000.
[19] N. Smick, B. LaBombard, C.S. Pitcher, J. Nucl. Mater. 337-339 (2005) 281.
[20] C.J. Boswell, J.L. Terry, B. LaBombard, B. Lipschultz, C.S. Pitcher, Plasma Phys. Control. Fusion 46 (2004) 1247.
[21] B. LaBombard, et al., Nucl. Fusion 44 (2004) 1047.
[22] S. Gangadhara, B. LaBombard, Plasma Phys. Control. Fusion 46 (2004) 1617.
[23] A. Loarte, et al., Phys. Plasmas. 18 (2011) 056105.
[24] A. Hubbard, et al., Multi-device studies of pedestal physics and confinement in the i-mode regime, presented at the 25th Fusion Energy Conference, St. Petersburg, Russia, 2014.